Sodium chloride precipitation reaction coefficient from crystallization experiment in a microfluidic device

Antoine Naillon, Pierre Joseph, Marc Prat

Sodium chloride precipitation reaction coefficient from crystallization experiment in a microfluidic device

A.Naillon[1,2], P.Joseph[2], M.Prat[1*]

[1]INPT, UPS, IMFT (Institut de Mécanique des Fluides de Toulouse), Université de Toulouse, Allée Camille Soula, F-31400 Toulouse, France and CNRS, IMFT, F-31400 Toulouse, France
[2]LAAS-CNRS, Université de Toulouse, CNRS, Toulouse, France

Abstract
The crystal growth of sodium chloride from an aqueous solution is studied from evaporation experiments in microfluidic channels in conjunction with analytical and numerical computations. The crystal growth kinetics is recorded using a high speed camera in order to determine the intrinsic precipitation reaction coefficient. The study reveals that the crystal growth rates determined in previous studies are all affected by the ions transport phenomena in the solution and thus not representative of the precipitation reaction. It is suggested that accurate estimate of sodium chloride precipitation reaction coefficient presented here offers new opportunities for a better understanding of important issues involved in the damages of porous materials induced by the salt crystallization.

Keywords:
A1. Evaporation
A1. Growth models
A1. Supersaturated solution
A1. Diffusion
B1. Sodium Chloride

1. Introduction

The crystallization of sodium chloride from an aqueous solution is a key phenomenon in relation with evaporation from porous media, [1], the generation of damages in buildings and monuments [2], or the injection of CO_2 in underground formations [3], to name only a few. The crystallization process is generally decomposed into two main steps: the nucleation step and the growth step. In this respect, it is important to distinguish the crystal growth kinetics [4] from the nucleation kinetics, which involves the induction time between the application of a supersaturation state and the appearance of the first crystals [5]. In the literature, they can both be found under the expression of "crystallization kinetics". In this paper, we focus on the crystal growth kinetics.

The crystal growth is studied within the framework of the diffusion reaction theory [6] (where other crystal growth theories: surface energy theory, adsorption layer theory and kinematic theory, are also presented). Crystal growth starts only once a stable nucleus, large enough to be stable, appears in the metastable solution. It relies on two coupled steps: an ion diffusion process from the solution to the crystal surface, followed by a reaction process where ions fit in the crystal lattice. These processes have been highlighted in refs. [7,8].

As illustrated in Fig. 1, the two steps occur in series and three zones can be defined. The first zone corresponds to a stagnant film (or adsorption layer) at the crystal-liquid interface. Far from the crystal, there is the bulk solution with a constant concentration. The concentration

* Corresponding author : mprat@imft.fr , +33 (0)5 34 32 28 83

increases following a diffusion law in the intermediate zone of size *d* between the crystal and the bulk.

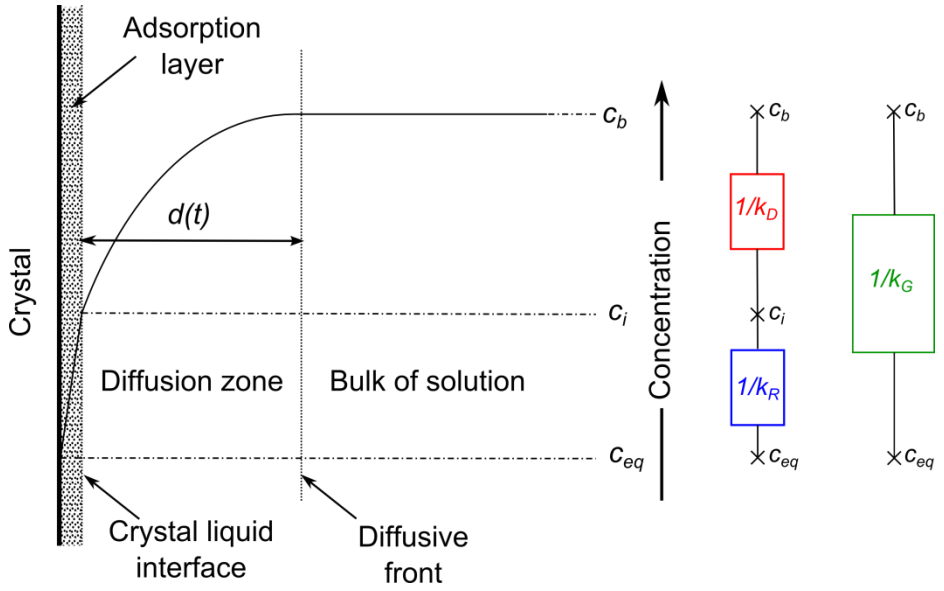

Fig. 1 *Modelling of crystal growth according to the reaction and diffusion theory. Three zones are defined depending on the evolution of the solute concentration: the stagnant film at the crystal/liquid interface, the bulk solution with a constant concentration far from the crystal, and in between, the diffusion zone of size d(t) where the concentration increases following a diffusion law. Adsorption layer and diffusion zone can be considered as two mass transfer resistances in series.*

The crystal growth rate, J (kg/m².s) in the adsorption zone and diffusion zone can be modelled as:

$$J_D = \frac{1}{A}\frac{dM}{dt} = k_D(c_b - c_i)\,, \tag{1}$$

$$J_R = \frac{1}{A}\frac{dM}{dt} = k_R(c_i - c_{eq})^n\,, \tag{2}$$

where M (kg) is the mass of the crystal, A is the crystal total surface, c_b (kg/m^3) is the bulk salt concentration of the solution, c_i is the salt concentration at the liquid crystal interface, and c_{eq} is the ion concentration at equilibrium; n is the order of the reaction and k_D and k_R (m/s) are the coefficients of mass transfer by diffusion and reaction, respectively. k_D can be seen as the ratio of the salt molecular diffusion coefficient D_s to the diffusion length d.
Considering the diffusion zone and the adsorption layer as two mass transfer resistances in series (as sketched in Fig.1) and for a first order reaction (n=1, which is the case for sodium chloride), an equation combining these two steps can be obtained,

$$J_G = \frac{1}{A}\frac{dM}{dt} = k_G\left(c_b - c_{eq}\right) \tag{3}$$

with

$$k_G = \frac{1}{\frac{1}{k_D} + \frac{1}{k_R}} = \frac{k_D k_R}{k_D + k_R}, \tag{4}$$

where k_G is referred to as the overall growth rate parameter. The equivalent of the mass transfer resistance is equal to the inverse of the growth rate parameter. In order to characterize the phenomenon driving the crystallization process, Garside [9] suggests to define the effectiveness factor for crystal growth η_r as the ratio between the overall growth rate and the growth rate obtained when the crystal surface is exposed to the bulk concentration:

$$\eta_r = \frac{J_G}{k_R (c_b - c_{eq})} \tag{5}$$

In other words, it is the ratio between the overall growth rate and the growth rate obtained when the crystallization is limited only by reaction, with an infinitely fast diffusion; η_r can be expressed as:

$$\eta_r = (1 - Da\eta_r) \tag{6}$$

where $Da = \frac{k_R}{k_D}$, is the Damkhöler number, which represents the ratio between the reaction flux and the mass transport flux. Thus

$$\eta_r = \frac{1}{1 + Da} \ . \tag{7}$$

Therefore, the process is controlled by diffusion when *Da* is large and η_r is low. On the contrary, it is controlled by reaction (the controlling process is the slowest one) when *Da* is small and η_r is large. Moreover, because NaCl crystal has a cubic shape, the mass precipitation rate can be related to the mean linear velocity of its faces w_{cr} (m/s) by (see Appendix A):

$$w_{cr} = \frac{dr}{dt} = \frac{J_G}{\rho_c} = \frac{k_G}{\rho_c}\left(c_b - c_{eq}\right) \tag{8}$$

where r is the half length of the side of a cubic crystal (m) and ρ_c is the crystal density (kg/m^3). In case of a spherical crystal or a growth in 1 dimension on both sides, Eq.(8) remains valid with r as the sphere radius or the crystal half length.

The above considerations clearly show that the crystal growth kinetics depends on both the local concentration c_i at the interface and coefficients k_D and k_R. The experiments typically allow determining w_{cr} (references are given below in the section on the results). Since both c_i and k_R are unknowns, it is clearly difficult to determine k_R from the experimental data. Also, as stated in [9], k_R is difficult to measure because it is hard to separate the reaction step from the diffusion one. In this context, the main objective of the paper is precisely to provide an accurate estimate of k_R.

It should be mentioned that correct values of k_R are of the uttermost importance for correctly evaluating the crystallization pressure, which is the key concept in relation with the damages caused by the salt crystallization in porous materials [10]. As explained in [11], what matters for evaluating the crystallization pressure is the salt concentration at the crystal surface when it becomes confined between the pore walls. This concentration is highly dependent on k_R (see [11] for more details).

2. Materials and methods

2.1 Experiments

Experiments are performed in microfluidic chips such as the one sketched in Fig. 2. It is composed of a large channel used for supplying the fluids: salt solution or gaseous nitrogen. Holes are drilled at both extremities to connect the chip to the external part of the experimental set-up. Channels of smaller cross section surface areas, referred to as pore channels, are designed perpendicularly to the supply channel. Two pore channel cross sections are used in order to study its influence on crystal shape: 5×5 µm² and 20×20 µm². For each cross section, three lengths are tested so as to consider different initial amounts of dissolved salt: 100 µm, 200 µm, 300 µm and 200 µm, 400 µm, 800 µm respectively.

The chips are made of polydimethylsiloxane (PDMS) and glass. First, a mold is fabricated in a clean room by standard photolithography using, however, a DF-1000 series dry film instead of a liquid photoresist as SU-8. Then, PDMS Sylgard 184 with a ratio of curing agent 1:10 is degassed under vacuum during 45 minutes, poured on the mold and cured at 80°C during 2 hours. It is unmolded after at least 20 minutes of cooling at ambient temperature. After unmolding, holes are made with bio punch and the chips are cut with a scalpel. Then a cover glass is bonded on the channel side thanks to smooth air plasma during 1 minute and 30 seconds. Finally, a second baking at 70°C during 30 minutes is done to ensure a good adhesion between glass and PDMS.

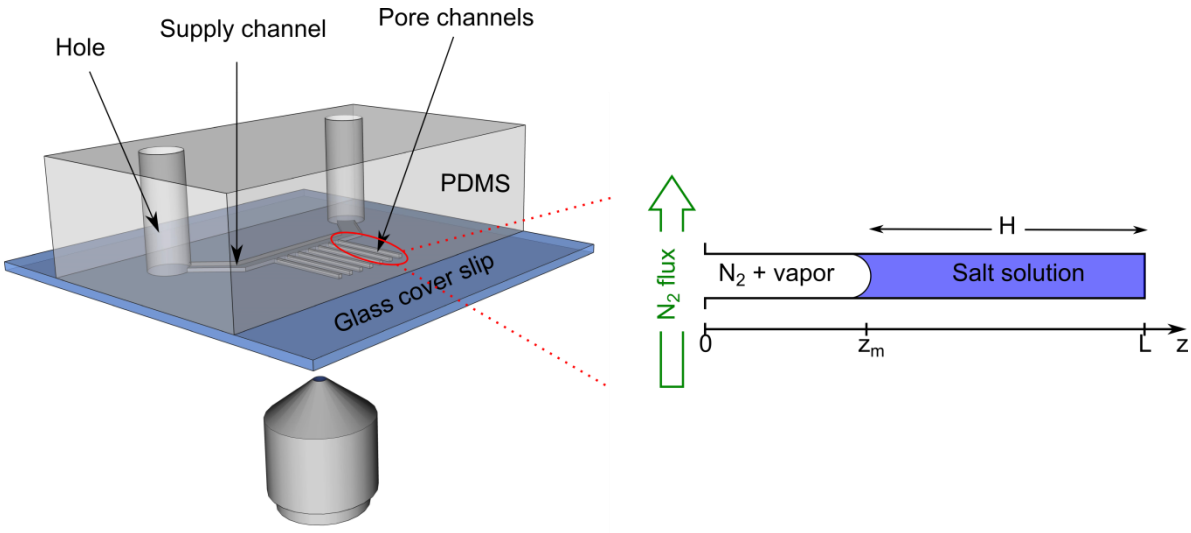

Fig. 2 *Scheme of the PDMS and glass microfluidic chip. The channels are casted on a mold fabricated with laminated photosensitive dry films (DF-series 1000), structured by photolithography. The crystallization is observed in the pore channels. First, salt solution is injected from the top hole through the supply channel and invades the pore channel. Once the device is filled, a N_2 flux is imposed from the bottom hole to empty the supply channel and isolate salt solution in the pore channel. This flux is maintained during all the experiment to evaporate the solution contained in the pore channels.*

The experiments are performed at room temperature (between 22 to 24°C) on an inverted microscope Zeiss Axio observer D1 working in transmission. The protocol is the following: capillary tubes (PTFE, 1/16 inch x 0.8 mm) link the chip to a pressure controller (Fluigent MFCS) managed by computer. One tube passes through a salt solution tank and the other not. The chip is filled from the top hole by salt solution with a known initial concentration. Once

the pore channels are filled, nitrogen is injected in the large channel from the bottom hole to push the solution out of this channel, leaving the pore channels filled. The gas flow is maintained during all the experiment to evaporate the salt solution in the pore channels (RH=0%).
Salt crystals form within the pore channels after evaporation of a sufficient amount of water for the ion concentration marking the onset of crystallization to be reached. Two video cameras are used: an Andor Zyla SCMos to record the kinetics of evaporation, with a low frame rate (between 1 and 2 seconds per image) and a large field, and a Photron Fastcam SA3 camera to record the kinetics of crystal growth at 500 or 1000 frames per second.
In order to perform the experiments with different amounts of dissolved salt in excess at nucleation, sodium chloride solution is prepared with two different molalities: 1.89 and 4.25 mol/kg, the saturation being 6.15 mol/kg (corresponding to mass fractions of 10%, 20% and 26.4 % respectively). Salt is provided by Sigma Aldrich, with a purity ensured to be higher than 99.5%. It is dissolved in deionized water.
Movies are exploiting thanks to the ImageJ© and Matlab© softwares to track the crystal liquid interface so as to determine the kinetics of crystal growth.
More details on the experimental setup are given in Appendix C.

2.2 Numerical simulations

A numerical model is developed and solved using the commercial software Comsol multiphysics 5.2© in order to analyze the experimental results. We focus on the beginning of the crystallization process over a very short period during which evaporation is negligible. Thus, this model is used to simulate the crystal growth of an initial nucleus in a solution when the crystal size is small compared to the size of the computational domain. For this reason, the problem is actually equivalent to the growth in an "infinite" domain. This means that the numerical domain is sufficiently large for the diffusive front of the dissolved salt concentration not to reach the domain boundary.
At initial time, the solution is supersaturated and a small nucleus is in the solution. Initial supersaturation S_0 (see below for a definition) is set to the mean experimental value (S=1.72, see below). We checked that the specified initial size of nucleus has not influence on final result. The transport of dissolved salt by diffusion and convection is taken into account as well as the crystal growth due to the precipitation reaction. The coefficient of mass transfer by reaction k_R is varied between 10^{-2} and 10^{-4} m/s so as to study its influence. The ion molecular diffusion coefficient D_s is taken equal to 1.3×10^{-9} m²/s.

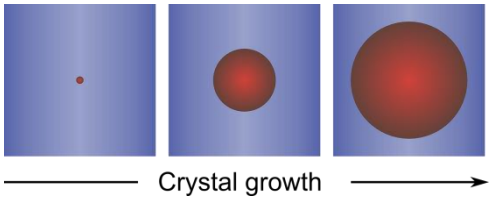

Fig. 3 *Sketch of the numerical simulation: a spherical crystal grows in a supersaturated solution in a domain of "infinite" size (only a little part of the domain is shown here).*

Technical details and equations are presented in Appendix D.

3. Results

3.1 Supersaturation at nucleation

The supersaturation of the solution is defined as

$$S=m/m_0 \tag{9}$$

where m (mol/kg) is the molality and subscript $_0$ refers to the reference state where the crystal is in equilibrium with the solution. As recalled in Appendix E, the molality can be determined from the solution concentration. A simple method to determine the salt concentration is to track the position of the receding meniscus in the pore channel at the onset of crystallization and to perform a simple mass balance. Knowing the initial volume V_0 of the salt solution of concentration c_0, the average concentration when the first crystal is detected on the images (nucleation), c_n, is given by:

$$c_n = c_{cr} = \frac{V_0}{V_n} c_0 \,, \tag{10}$$

where V_n is the volume of solution in the channel when the first crystal is detected on the images since the total amount of salt remains constant (only pure water evaporates).
An implicit hypothesis when using Eq.(10) is that the concentration is about the same everywhere in the solution. To validate this assumption, it is possible to define a Peclet number by the ratio between the ions production rate at the receding meniscus and the diffusion rate [12]:

$$Pe = \frac{\frac{dz_m}{dt} H}{D_s}, \tag{11}$$

z_m represents the position of the meniscus (distance to the channel entrance) and H is the length of the liquid part (see Fig.2). The assumption of uniform concentration is valid only if the Pe number is much lower than 1 (low evaporation rate in comparison with the diffusion velocity), which is always the case in our experiment. Using Eq.(11) leads to Pe=0.08±0.07 taking into account all the experiments, indicating that assuming the concentration as uniform is reasonable.

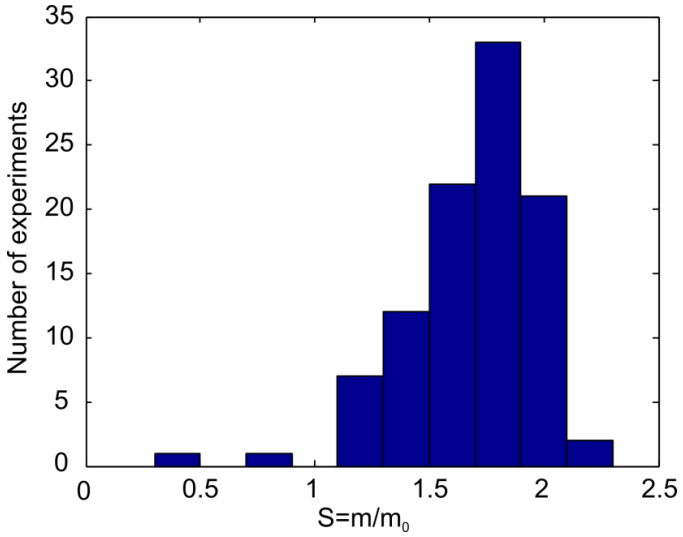

Fig. 4 *Histogram of supersaturation values at nucleation for the 99 experiments. Two values are non-consistent because they are lower than 1. In the two corresponding experiments, liquid films seem to be trapped in front of the receding meniscus and nucleation occurs in the films. The assumption of uniform concentration through the solution is not valid in this case. As shown in* [14] *and also discussed in* [15]*, evaporation takes place at the film tips and the convective flux within the film is not negligible. Our definition of Peclet number is then non valid anymore. Taking out these 2 values, the mean supersaturation is equal to S=1.72.*

The value of supersaturation is measured in 99 experiments (Fig. 4). The mean value is found to be equal to *S=1.72*, which is consistent with previous studies [12-13]. No dependence with pore channel length, depth or initial concentration is noticed.

3.2 Crystallization kinetics

The crystallization kinetics is recorded over very short periods (between 0.1 and 2 seconds) at 1000 frames per second. Pictures from three experiments of crystal growth are shown in Fig. 5*a*. The kinetics of crystal growth is extracted by tracking the liquid crystal interface in the main growth direction (black line in Fig. 5*a*). Note that the crystallization kinetics is studied from the images obtained using the high speed camera. The latter has a much smaller field of view compared to the low frame rate camera. As result, this is not 99 experiments as for the supersaturation study but only 10 which have been considered for studying the kinetics.

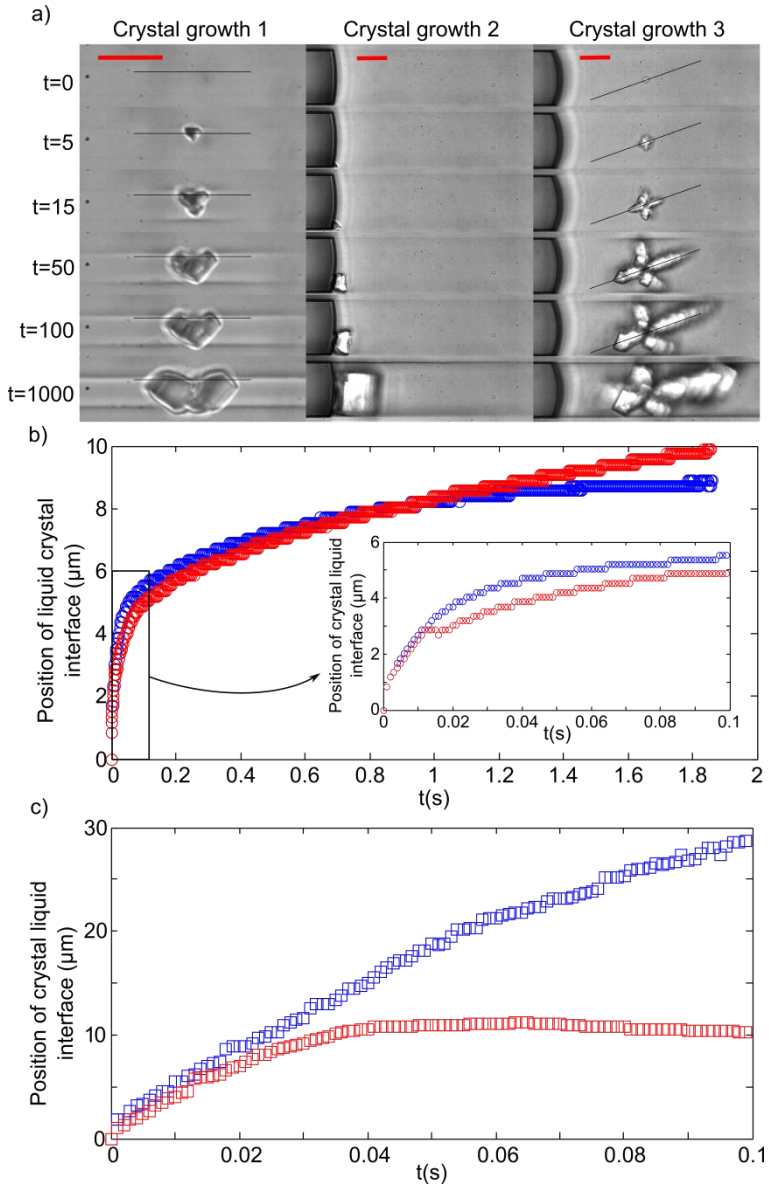

Fig. 5 *a) Pictures of crystal growth in pore channels. The black lines show the direction along which the kinetics of crystal growth is measured. Red scale bar represents 10 µm; Time is in millisecond; b) and c) represent the kinetics of crystal growth corresponding to 1 and 3 of a) respectively. The position of liquid crystal interface as a function of time is shown in blue in the right direction and in red in the left direction. The insert in b) focuses on the first 100 ms. In c), the kinetics of growth is not extracted after 100 ms because the crystal rotates in the channel.*

As illustrated in Fig. 5b, two steps in the crystal growth can be distinguished: a very fast one over a period of about 10-100 ms, with a quasi-constant kinetics (the crystal surface moves linearly), and a second one characterized by a decreasing kinetics (the liquid-crystal interface slows down).

The shape of the crystal depends on the channel size and on the location of the nucleation. When the crystal appears far from the liquid air interface, a "cubic" crystal is observed in the 5×5 µm² channel (Fig. 5a, "Crystal growth 1") whereas a "star" crystal is observed in the 20×20 µm² channel (Fig. 5a, "Crystal growth 3"). The latter can be referred to as a Hopper crystal [13]. When the crystal appears on the liquid gas interface, it is directly confined between the channel wall and the liquid-gas interface (Fig. 5a, "Crystal growth 2"). These

cases are discarded to determine the kinetics of growth because we assume that it is influenced by the geometrical confinement. In other terms, we consider that the transport of ions in the wedge formed by the liquid-air interface and the channel wall is different from the situation considered in the theoretical and numerical approaches (see Sections 2.2 and 4) where the crystal grows in the middle of a solution.
It appears that the crystal growth is very fast at the onset of crystallization, much faster than the fastest kinetics reported in previous studies. For example, a liquid-crystal interface velocity d*r*/d*t* of around 10 µm/s is reported in [16]. However, the low camera rate acquisition (0.5 frames per second) used in [16] does not allow to measure the beginning of the growth. Here, thanks to the high speed camera, we can focus on the first milliseconds when the kinetics of crystal growth is constant. The crystal growth velocity dr/dt is estimated after 10 ms for all the experiments, when the crystal has still a compact shape. This leads to a mean value equal to $dr/dt = 271 \pm 62$ µm/s (the mean value and its standard deviation are calculated considering the 10 experiments and the growth on each side of crystal). It is convenient to express the growth kinetics in term of the overall growth parameter k_G in order to compare our data with values from previous experiments. k_G is computed using Eq. (8) with c_b corresponding to the concentration at the onset of crystallization. This gives $k_G = 2.33\times10^3 \pm 0.1\times10^3$ µm/s.

4. Discussion

As mentioned before, the crystal growth kinetics observed in our experiments is much faster than in previous experiments. In order to compare with our values, we have extracted the kinetics of sodium chloride crystal growth from different previous papers. The kinetics is expressed in term of k_G, thanks to Eq. (8). Values are presented in Table 1 (the determination of k_G for each reference is presented in the Appendix F).

Ref	Sursaturation - *S*	k_G (µm/s)	Time of measurement
[17]	1.011 - 1.044	11.77 ± 1.1	\
[12]	1.62	10.3	5 min
[18]	1.93 - 1.98	23.4 ± 2.7	20 s
[16]	1.3	126	2 s
This study	1.476 – 2.118	$2.33\times10^3 \pm 0.1\times10^3$	10 ms

Table 1 *Values of the overall growth parameter k_G of sodium chloride found in the literature, and comparison with this study. The time of measurement corresponds to the time at which the mean experimental growth velocity is measured. It is difficult to define this time for ref* [17]. *It is clear that the lower the time of measurement, the higher the overall growth parameter. Determination of k_G for each reference is presented in Appendix F.*

The time of measurement corresponds to the time t_m used to calculate the velocity experimentally, i.e. from Eq.(8)

$$w_{cr} = \frac{dr}{dt} \approx \frac{r(t_m) - r(0)}{t_m} = \frac{k_G}{\rho_c}\left(c_b - c_{eq}\right) \tag{12}$$

As can be seen from Table 1, the value of k_G=2.33 mm/s after 10 ms from our experiments is 20 to 500 times higher than the values extracted from the literature. Table 1 makes clear that the overall growth rate parameter depends on the duration of the experiment. In particular, the

lower the time of velocity integration, the higher the growth rate parameter. We can explain this result with the variation of the coefficient of mass transfer by diffusion, k_D, with time. According to the diffusion reaction theory, the coefficient of mass transfer by reaction, k_R, is an intrinsic property of the crystal whereas k_D depends on a diffusive length which evolves in time. This can be illustrated from a simple model of the crystal growth in one dimension controlled only by diffusion, i.e. assuming a very large k_R. The corresponding problem with boundary condition 1 is sketched in Fig. 6.

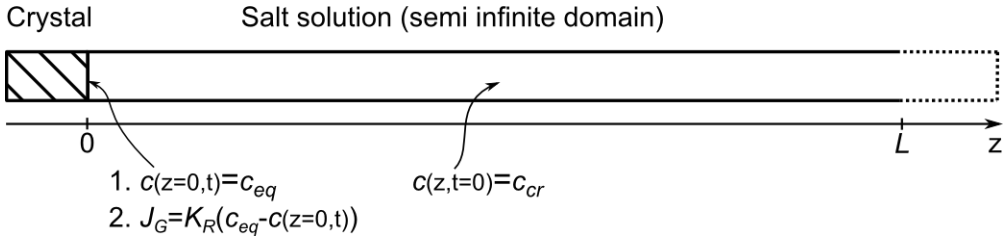

Fig. 6 *Sketch of the crystal growth model in 1 dimension. At initial time, the salt concentration is uniform in the solution. Two different cases are modelled depending on the boundary condition at the crystal solution interface. Case 1: fixed concentration at the interface equal to the equilibrium concentration, which corresponds to the case where k_R tends to infinity. Case 2: fixed resistance to mass transfer by reaction; c_{cr} is the ion concentration at the onset of crystallization (supersaturation)*

In this model, the convection induced by the crystal liquid interface motion is not taken into account. The solution for a semi-infinite domain is used because of its simplicity in comparison to the case of a finite domain. This approximation is correct if the diffusive front which starts from the crystal has not the time to reach the other boundary (end of pore channels in our experiments). In other words, the two solutions are equivalent for times much lower than the diffusive time, $t_D=L^2/D_s$, where L is the length of the considered finite domain (for instance, if L=1mm, t_D=769s). The solution to this problem is given in [19]:

$$\frac{c(z,t)-c_{eq}}{c_{cr}-c_{eq}} = \mathrm{erf}\left(\frac{z}{2\sqrt{\mathrm{D_s t}}}\right) \tag{13}$$

where $c_{cr}=c_n=c_b$ is the ion concentration at the onset of crystallization (thus corresponding to the supersaturation). From Eq.(13) we can express the velocity of crystal growth controlled only by diffusion as:

$$w_{cr,D} = \frac{dr}{dt} = \frac{D_s}{\rho_{cr}}\left(\frac{\partial c}{\partial z}\right)_{z=0} = \frac{(c_{cr}-c_{eq})}{\rho_{cr}}\sqrt{\frac{D_s}{\pi t}} \tag{14}$$

The mean velocity of crystal growth between nucleation (t=0) and a time t_m is then obtained integrating Eq.(14) over the duration t_m:

$$w_{cr,D,mean} = \frac{r(t_m)}{t_m} = \frac{2(c_{cr}-c_{eq})}{\rho_{cr}}\sqrt{\frac{D_s}{\pi t_m}} \tag{15}$$

Combining Eqs. (15) and (8) leads to the following theoretical evolution of k_G as a function of measurement time t_m:

$$k_G = k_D = 2\sqrt{D_s/\pi t_m} \tag{16}$$

This law is plotted in Fig. 7 together with the values of k_G reported in Table 1. As can be seen from Fig.7, the value of k_G found in the literature varies as $t^{-0.494}$, which is very close to the theoretical prediction $t_m^{-0.5}$. This is a first indication that the crystal growth in the aforementioned experiments is controlled by diffusion.

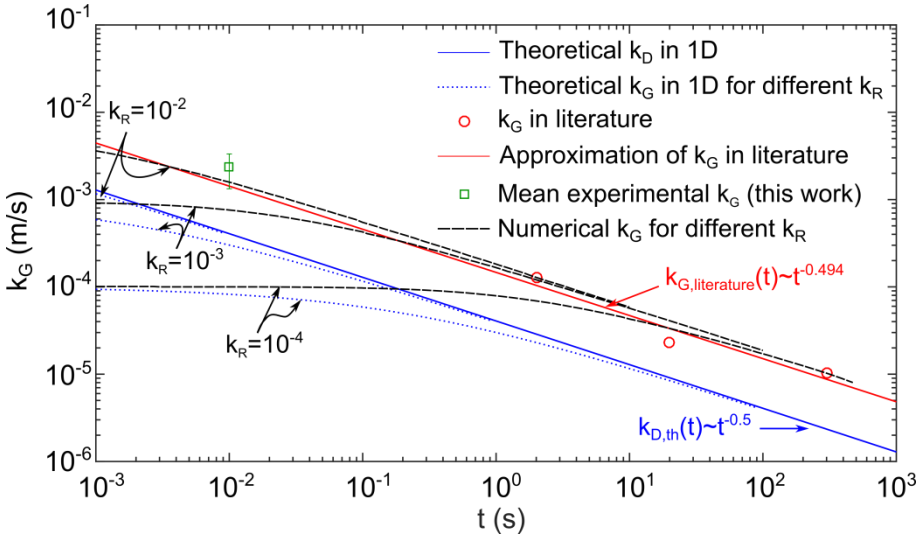

Fig. 7 *Variation of the overall coefficient of crystal growth depending on the duration of growth. The blue dotted lines correspond to the theoretical variation of k_G for different k_R (see text). The blue solid line is the theoretical value assuming an infinite value for k_R, thus k_G=k_D. The red circles correspond to values of k_G found in literature. The dashed lines are numerical computation results for different values of k_R. The solid red line corresponds to a power law fit of literature points. The green square corresponds to our experimental points after 10 ms.*

Proceeding similarly, it is interesting to take into account the reaction step. The crystal growth in one dimension controlled by diffusion and reaction is modelled as sketched in Fig. 6. This means using boundary condition 2 (Fig. 6). The solution of this problem is again given in [19]:

$$\frac{c(z,t)-c_{cr}}{c_{eq}-c_{cr}} = \operatorname{erfc}\left(\frac{z}{2\sqrt{D_s t}}\right) - \exp(hz + h^2 D_s t)\operatorname{erfc}\left[\frac{z}{2\sqrt{D_s t}} + h\sqrt{D_s t}\right] \tag{17}$$

where h=k_R/D_s. The velocity of crystal growth controlled by diffusion and reaction and its average value are given by:

$$w_{cr,RD} = \frac{dr}{dt} = \frac{D_s}{\rho_{cr}}\left(\frac{\partial c}{\partial z}\right)_{z=0} = k_R\frac{(c_{cr}-c_{eq})}{\rho_{cr}}\exp(h^2 D_s t)\operatorname{erfc}\left(h\sqrt{D_s t}\right) \tag{18}$$

$$w_{cr,RD,mean} = \frac{(c_{cr} - c_{eq})}{\rho_{cr}} \left[\frac{\exp(h^2 D_s t_m)\,\mathrm{erfc}\left(h\sqrt{D_s t_m}\right)}{h t_m} - \frac{1}{h t_m} + 2\sqrt{\frac{D_s}{\pi t_m}} \right] \quad (19)$$

Combining Eqs. (8) and (19), the theoretical evolution of k_G as a function of measurement time can be expressed as

$$k_G = \left(\frac{\exp(h^2 D_s t_m)\mathrm{erfc}\left(h\sqrt{D_s\ t_m}\right)}{h t_m} - \frac{1}{h t_m} + 2\sqrt{\frac{D_s}{\pi t_m}} \right) \quad (20)$$

This law is plotted in blue dotted line for different values of k_R in Fig. 7. As can be seen, the kinetics of crystal growth follows the diffusive law for a measurement time of 10 ms only if the coefficient of mass transfer by reaction is bigger than 10^{-3} m/s.
Since Eq.(20) gives the solution in 1D using a linear Cartesian coordinate and for a fixed crystal – solution interface, numerical simulations are performed to extract the kinetics of growth for different values of k_R=10^{-4}, 10^{-3} and 10^{-2} m/s for conditions closer to the experimental situation (moving crystal – solution interface in a 3D domain). The numerical results for k_G are compared with the experimental and theoretical ones in Fig.7. As can be seen, Fig.7 shows a very good agreement between the experimental and the numerical results. The difference with the theoretical values from the 1D solution is about of a factor 4, which can be explained by the fact that the numerical simulations (and the experiments) correspond to a growth in a 3D domain whereas the theoretical solution is developed only in 1 dimension. In addition, the theoretical solution does not take into account the motion of the crystal solution interface.
Therefore, the conclusion is that the crystal growth is only controlled by diffusion in all of the mentioned papers. Thus $k_G = k_D$ in those experiments and the data are not sufficient to extract k_R. Consequently, *Da* is large and η_r is low in all these experiments.
Concerning the dependence of k_G on k_R, the numerical simulation confirms that the crystal growth is limited by diffusion after 10 ms only if the parameter of crystal growth by reaction k_R is larger than 10^{-3} m/s. This result allows us to propose as a lower bound $k_R = 2.3\times10^{-3}$ m/s, which is the kinetics we measure as reported in Section 4.

5. Summary and conclusions

In this study, we present a microfluidic device allowing the accurate observation of sodium chloride crystal growth from a supersaturated solution. A frequency of acquisition as high as 1000 Hz is employed. This gives the possibility of studying the crystal growth in the regime controlled by the reaction. To the best of our knowledge, it is the first time that the kinetics of crystal growth is measured in the early stage of the growth where the growth is not controlled only by the ion transport phenomena toward the crystal but also by the precipitation reaction. This enables us to propose a new order of magnitude for the coefficient of mass transfer by reaction: $k_R > 2.3\times10^{-3}$ m/s, ten to hundred times higher than the values used in literature. The comparison with analytical and numerical simulation results highlight that the difference comes from the averaging time of measurement. When it is too long, the crystal growth is controlled by diffusion and not by reaction and the value of the reaction coefficient k_R cannot be deduced from the experimental data.
Similar experiments could be performed with other salts so to make a new data bank of the coefficient of mass transfer by reaction. To mention only one application, correct values of k_R are crucial for determining the crystallization pressure responsible of the generation of

damages due to crystallization in porous materials. Accordingly, the variability of k_R with the salt nature could contribute to explain why some salts cause more damages than others.
Finally, the study illustrates one more time the effectiveness of microfluidic devices for characterizing chemical or physical properties.

Acknowledgements: Financial supports from ANDRA, INSIS-CNRS and CNRS NEEDS-MIPOR program are gratefully acknowledged. This work was partly supported by LAAS-CNRS micro and nano technologies platform member of the French RENATECH network.

Appendix A. Relation between the overall crystal growth rate J_G and the mean linear velocity of its faces w_{cr} (m/s)

Considering a sodium chloride cubic crystal and taking r, the half length of its side as the reference length, the mass variation of the crystal can be expressed as:

$$\frac{dM}{dt} = \rho_{cr}\frac{dV}{dt} = \rho_{cr}\frac{d(2r)^3}{dt} = \rho_{cr}6(2r)^2\frac{dr}{dt} = \rho_{cr}A_{cr}\frac{dr}{dt}, \tag{A1}$$

where A_{cr} is the surface of the crystal. Combined with Eq.(3), we obtain the relationship (Eq.(8) in the text):

$$w_{cr} = \frac{dr}{dt} = \frac{J_G}{\rho_{cr}} = \frac{k_G}{\rho_{cr}}\left(c_b - c_{eq}\right), \tag{A2}$$

Appendix B. Relation between volume ratio and concentration

The salt mass conservation during evaporation implies:

$$c_n V_n = V_0 c_0 , \tag{B1}$$

Index $_n$, refers to the time of nucleation and $_0$ the initial time. It gives:

$$x_{s,n}\rho_{l,n} = \frac{V_0}{V_n}x_{s,0}\rho_{l,0} . \tag{B2}$$

Using the relation between salt mass fraction and salt solution density given in [15]: $\rho_l = \frac{\rho_w}{1-0.7\,x_s}$, we find:

$$\frac{x_{s,n}\rho_w}{1-0.7x_{s,n}} = \frac{V_0}{V_n}\frac{x_{s,0}\rho_w}{1-0.7x_{s,0}} . \tag{B3}$$

As a result, it is obtained that:

$$x_{s,n} = \frac{x_{s,0}}{\frac{V_n}{V_0} + 0.7x_{s,0}\left(1-\frac{V_n}{V_0}\right)} , \tag{B4}$$

Appendix C. Fabrication of experimental devices

As sketched in Fig.1, experiments are performed on a microfluidic chip made of glass and PDMS.

a. Mold fabrication

Molds are made for channel of 5×5 µm² cross section with DF-1005 and for channel of 20×20 µm² cross section with DF-1020 respectively. They are made in a clean room by standard photolithography, excepted that photoresist is a dry film DF-1000 series. The silicon wafer surface is first cleaned and activated in an O_2 plasma (Tepla 300) during 5 minutes with a power of 400 W and under a pressure equal to 1.5 mbar.
Then, the dry films are laminated with laminator Shipley 3024 under a pressure of 2.5 bar, a temperature of 100°C and with a velocity of 0.5 m/min.
DF-1005 and DF-1020 are exposed to an energy density equal to 160 mJ/cm² and 200 mJ/cm² respectively through a quartz mask. After exposure, the wafer is baked at 100°C during 3 or 5 minutes and developed in a solution of cyclohexanone during 3 or 4 minutes. A hard bake is performed at the end at 125°C during 2 minutes.
To avoid the PDMS adhesion on the mold during the casting and curing steps, the mold is rendered hydrophobic. It is immersed in a bath of 50 ml of xylene and 0.5 ml of OTS (using this solution under a nitrogen inert atmosphere is better to avoid the OTS oxidation).

b. Fabrication of PDMS chip

PDMS Sylgard 184 with a ratio of curing agent 1:10 is degassed under vacuum during 45 minutes, poured on the mold and cured at 80°C during 2 hours. It is unmolded after at least 20 minutes of cooling at ambient temperature.
After unmolding, holes are made with bio punch of 1 mm diameter and the chips are cut with a scalpel.
Then a 125 µm thick cover glass is bonded on the channel side thanks to smooth air plasma (Diener Pico) during 1 minute and 30 seconds under a pressure of 0.4 mbar and with a power of 200 W.
Finally, a second baking at 70°C during 30 minutes is done to ensure a good adhesion between glass and PDMS.

Fig. A1 *Picture of the PDMS experimental chip. The PDMS is bonded on a glass cover slip.*

Appendix D. Numerical Models

The numerical simulations are performed with Comsol Multiphysics 5.2©, a commercial software based on the finite element method. The crystal shape is spherical. In an infinite domain, this leads to consider a 1D problem using spherical coordinates. At initial time, the solution is supersaturated and a small nucleus is in the solution. It is checked after the simulation that initial size of nucleus has not influence on final result.
Before describing the mathematical model, it is useful to define some terms. Indeed, considering the salt solution (subscript $_l$) as a binary mixture composed of dissolved salt (subscript $_s$) and water (subscript $_w$), and considering that the crystal (subscript $_{cr}$) interface moves at the velocity w_{cr}, we can define:

- In term of species concentration:
  - c_i (kg.m^{-3}): mass concentration of specie i: $c_i = \frac{M_i}{V_l}$;
  - ρ_l (kg.m^{-3}): solution density: $\rho_l = c_s + c_w$;
  - x_i : mass fraction of specie i: $x_i = \frac{c_i}{\rho_l}$;
  - ρ_{cr} (kg.m^{-3}): crystal density;
- In term of species transport in the solution:
  - $\boldsymbol{v_i}$ (m.s^{-1}): velocity of specie i. Note that each species has a different velocity in the mixture;
  - $\boldsymbol{v_l}$ (m.s^{-1}) : velocity of the mixture: $\boldsymbol{v_l} = \frac{c_s \boldsymbol{v_s} + c_w \boldsymbol{v_w}}{\rho_l}$;
  - $\boldsymbol{J_i}$ (kg.m^{-2}.s^{-1}) : mass flux of specie i in the fixed frame: $\boldsymbol{J_i} = c_i \boldsymbol{v_i}$;
  - $\boldsymbol{j_i}$ (kg.m^{-2}.s^{-1}) : relative mass flux of specie i in the relative frame moving at velocity $\boldsymbol{v_l}$: $\boldsymbol{j_i} = c_i(\boldsymbol{v_i} - \boldsymbol{v_l})$;
- In term of flux through a moving interface:
  - $\boldsymbol{w_j}$ (m.s^{-1}): velocity of interface j.
  - $\boldsymbol{\phi_i}$ (kg.m^{-2}.s^{-1}) : mass flux of specie i through the moving interface j: $\boldsymbol{\phi_i} = c_i(\boldsymbol{v_i} - \boldsymbol{w_j})$;

The problem is modelled mathematically as follows. The continuity equation for the mixture, the momentum equation and the species continuity (NaCl) equation are expressed as:

$$\frac{\partial \rho_l}{\partial t} + \nabla . \rho_l \boldsymbol{v_l} = 0 \tag{D1}$$

$$\rho_l \left[\frac{\partial \boldsymbol{v_l}}{\partial t} + \boldsymbol{v_l} \nabla . \boldsymbol{v_l} \right] = -\nabla P_l + \mu_l \nabla^2 \boldsymbol{v_l} \tag{D2}$$

$$\frac{\partial \rho_l x_s}{\partial t} + \nabla . (\rho_l x_s \boldsymbol{v}_l) = \nabla . (\rho_l D_s \nabla x_s) \tag{D3}$$

Equation D3 is written considering that the salt flux is composed of a convective contribution and a diffusive one:

$$\boldsymbol{J_s} = c_s \boldsymbol{v_l} + \boldsymbol{j_s} = c_s \boldsymbol{v_l} - \rho_l D_s \nabla x_s \tag{D4}$$

The interface conditions at the crystal-liquid interface are expressed as follows. Two conditions can be derived. The first one expresses that water cannot cross this interface:

$$\boldsymbol{\phi_w} . \boldsymbol{n_{cr}} = c_w(\boldsymbol{v_w} - \boldsymbol{w_{cr}}) . \boldsymbol{n}_{cr} = [c_w \boldsymbol{v_l} - \rho_l D_s \boldsymbol{\nabla} x_w - c_w \boldsymbol{w_{cr}}] . \boldsymbol{n_{cr}} = 0 \, . \tag{D5}$$

Replacing x_w with 1-x_s and c_w with ρ_l-c_s gives:

$$[c_s \boldsymbol{v_l} - \rho_l D_s \boldsymbol{\nabla} x_s]. \boldsymbol{n_{cr}} = [\rho_l \boldsymbol{v_l} - (\rho_l - c_s)\boldsymbol{w_{cr}}]. \boldsymbol{n_{cr}} \quad \text{(D6)}$$

where $\boldsymbol{n_{cr}}$ is the unitary vector normal to the interface, pointing towards the liquid. The second condition expresses the mass conservation of salt. The mass flux of dissolved salt crossing the interface corresponds to the mass variation of the crystal:

$$(\boldsymbol{\phi_s} + \rho_{cr}\boldsymbol{w_{cr}}). \boldsymbol{n_{cr}} = [c_s(\boldsymbol{v_s} - \boldsymbol{w_{cr}}) + \rho_{cr}\boldsymbol{w_{cr}}]. \boldsymbol{n_{cr}} = 0\ . \quad \text{(D7)}$$

And the boundary condition for the salt flux is obtained using Eq. (D4) in Eq.(D6):

$$[c_s \boldsymbol{v_l} - \rho_l D_s \boldsymbol{\nabla} x_s]. \boldsymbol{n_{cr}} = -(\rho_{cr} - c_s)\boldsymbol{w_{cr}}. \boldsymbol{n_{cr}} = \boldsymbol{J_s}. \boldsymbol{n_{cr}}. \quad \text{(D8)}$$

The condition of salt solution velocity is obtained by adding Eqs. (D6) and (D7). This yields:

$$\boldsymbol{v_l}. \boldsymbol{n_{cr}} = \left(1 - \frac{\rho_{cr}}{\rho_l}\right) \boldsymbol{w_{cr}}. \boldsymbol{n_{cr}} \quad \text{(D9)}$$

Finally, $\boldsymbol{w_{cr}}$ is given by Eq. (8):

$$w_{cr} = \frac{k_r}{\rho_c}\left(c - c_{eq}\right)\ . \quad \text{(D10)}$$

The robustness of the model is done by checking the mass conservation of salt in the entire domain (solution + crystal). It can be noted that it is more difficult for the solver to converge for simulations performed for the highest value of k_R=10^{-2} m/s because of the higher kinetics of fluid motion and mesh deformation.

Appendix E. Relation between mass fraction, mass concentration and molality

Study of crystal growth involves determining the amount of ions in solutions. The mixture composition can be expressed using various definitions such as mass fraction, mass concentration or molality. The variable choice differs from one paper to the other. The following defines each variable and recalls the link between them. These relations are used in the next section to express of the overall growth rate parameter found in different papers in the same units.
Subscript $_l$, refers to the salt solution, which is a binary mixture composed of dissolved salt (subscript $_s$) and water (subscript $_w$).

c. Definition

- Mass concentration, c_i (kg.m^{-3}):

$$c_i = \frac{\text{mass of specie i}}{\text{volume of solution}} = \frac{M_i}{V_l}\ , \quad \text{(E1)}$$

- Mass fraction, x_i (∅):

$$x_i = \frac{\text{mass of specie i}}{\text{mass of solution}} = \frac{M_i}{M_l} = \frac{c_i}{\rho_l}, \quad \text{(E2)}$$

- Molality, m_i (mol.[kg of solvent]$^{-1}$):

$$m_i = \frac{\text{mole of specie i}}{\text{mass of free solvant}} = \frac{n_i}{M_{solvant}}, \quad \text{(E3)}$$

- Supersaturation, S (∅):

$$S = \frac{\text{molality}}{\text{equilibrium molality}} = \frac{m}{m_{eq}}, \quad \text{(E4)}$$

d. **Useful relationships**

- We use the following relationship between the density of a NaCl solution and the salt mass fraction or mass concentration [15]:

$$\rho_l = \frac{\rho_w}{(1 - 0{,}7x_s)} = \frac{\rho_w}{\left(1 - 0{,}7\frac{c_s}{\rho_l}\right)} = \rho_w + 0{,}7c_s, \quad \text{(E5)}$$

where ρ_w is the density of pure water

- Relationship between solution density and solute mass concentration:

$$\rho_l = c_s + c_w, \quad \text{(E6)}$$

- Relationship between salt molality and salt mass concentration:

$$m_s = \frac{n_s}{M_w} = \frac{c_s}{\mathbf{M_s} c_w} = \frac{c_s}{\mathbf{M_s}(\rho_l - c_s)} = \frac{c_s}{\mathbf{M_s}(\rho_w - 0{,}3\ c_s)}, \quad \text{(E7)}$$

where $\mathbf{M_s}$ is the molar mass of salt. Conversely:

$$c_s = \frac{m_s \mathbf{M_s} \rho_w}{1 + 0{,}3 m_s \mathbf{M_s}}, \quad \text{(E8)}$$

Appendix F. Determination of the overall growth rate parameters reported in Table 1

In order to compare values of the overall crystal growth rate parameter from different sources, we have expressed values of crystal growth found in other papers using the same convention as in the present study. Results are presented below:

Ref [17]:

Article data		Result		
$\overline{x_{cr}} - \overline{x_{eq}}$ (g/ 100g H_20)	*d(2r)/dt* (m/s)	c_{cr} (kg/m^3)	J_G (kg/m²/s)	k_G (m/s)
0.4	4.20×10^{-8}	327.7	4.55×10^{-5}	1.40×10^{-5}
0.6	5.60×10^{-8}	329.31	6.06×10^{-5}	1.24×10^{-5}
0.8	7.00×10^{-8}	330.93	7.58×10^{-5}	1.16×10^{-5}
1	8.50×10^{-8}	332.55	9.20×10^{-5}	1.13×10^{-5}
1.2	1.00×10^{-7}	334.17	10.8×10^{-5}	1.11×10^{-5}
1.4	1.16×10^{-7}	335.79	12.6×10^{-5}	1.10×10^{-5}
1.6	1.31×10^{-7}	337.41	14.1×10^{-5}	1.09×10^{-5}

Table F1 *Data from* [17] *used to determine* k_G.

c_{cr} is obtained noting that $m_{cr} = \overline{x_{cr}}/100/\boldsymbol{M_s}$ and using Eq. (E8) which gives :

$$c_{cr} = \frac{\overline{x_{cr}}\rho_w}{100 + 0.3 \times \overline{x_{cr}}} \tag{F1}$$

J_G is obtained using Eq.(A2) and k_G using Eq. (3).

Ref [12]:

In this paper the mean kinetics of crystal growth during the first five minutes is equal to 1.6 µm/s.

Article data		Result		
$S\ (m/m_0)$	*d(2r)/dt* (m/s)	c_{cr} (kg/m^3)	J_G (kg/m²/s)	k_G (m/s)
1.62	1.60×10^{-6}	492	1.73×10^{-3}	1.03×10^{-5}

Table F2 *Data from* [12] *used to determine* k_G.

Ref [18]:

Article data		Results		
m	*d(2r)/dt* (m/s)	c_{cr} (kg/m^3)	J_G (kg/m²/s)	k_G (m/s)
11.9	5.30×10^{-6}	575	5.74×10^{-3}	2.29×10^{-5}
12.2	5.10×10^{-6}	587	5.52×10^{-3}	2.10×10^{-5}
11.36	5.60×10^{-6}	554	6.06×10^{-3}	2.64×10^{-5}

Table F3 *Data from* [19] *used to determine* k_G.

Ref [16]:

Authors indicate that the growth rate is about 10μm/s and the supersaturation is about 1.3. With these approximate values, one obtains the values reported in Table F4.

Article data		Result		
M_{cr} (mol/l)	$d(2r)/dt$ (m/s)	c_{cr} (kg/m^3)	J_G (kg/m²/s)	k_G (m/s)
7.03	10×10^{-6}	410	10.82×10^{-3}	1.26×10^{-4}

Table F4 *Data from* [16] *used to determine* k_G.

References

1 S. Veran-Tissoires, M. Prat, Evaporation of a sodium chloride solution from a saturated porous medium with efflorescence formation, J. Fluid Mech. **749** (2014) 701–749.

2 A. S. Goudies and H. A. Viles, *Salt Weathering Hazards*, Wiley, Chichester, 1997.

3 M. Kim, A. Sell, D. Sinton, Aquifer-on-a-Chip: understanding pore-scale salt precipitation dynamics during CO2 sequestration, Lab Chip **13** (2013) 2421–2662.

4 A. E. Nielsen and J. M. Toft, Electrolyte crystal growth kinetics, J. Cryst. Growth **67** (1984) 278–288.

5 R. Grossier, Z. Hammadi, R. Morin, S. Veesler, Predictive Nucleation of Crystals in Small Volumes and Its Consequences, Phys. Rev. Lett., **107**, (2011) 025504.

6 J. W. Mullin, *Crystallization*, Elsevier, 4th editio., 2001.

7 A. A. Noyes, W. R. Whitney, Rate of solution in solid substances in their own solution, J. Am. Chem. Soc., **19** (1897) 930–934.

8 A. Berthoud, Théorie de la formation des faces d 'un cristal, J. Chim. Phys. **10** (1912) 624–635.

9 J. Garside, The Concept of effectiveness factors in crystal growth, Chem. Eng. Sci. **26** (1971) 1425–1431.

10 G. W. Scherer, Stress from crystallization of salt, Cem. Concr. Res., **34** (2004) 1613–1624.

11 A. Naillon, P. Joseph, M. Prat, Ion transport and precipitation kinetics as key aspects of the stress generation on pore walls induced by sodium chloride crystallization, to be submitted.

12 A. Naillon, P. Duru, M. Marcoux, M. Prat, Evaporation with sodium chloride crystallization in a capillary tube, J. Cryst. Growth **422** (2015) 52–61.

13 J. Desarnaud, H. Derluyn, J. Carmeliet, D. Bonn, N. Shahidzadeh, Metastability limit for the nucleation of NaCl crystals in confinement, J. Phys. Chem. Lett. **5** (2014) 890–895.

14 F. Chauvet, P. Duru, S. Geoffroy, M. Prat, Three periods of drying of a single square capillary tube, Phys. Rev. Lett. **103** (2009) 124502.

15 B. Camassel, N. Sghaier, M. Prat, S. Ben Nasrallah, Evaporation in a capillary tube of square cross-section: application to ion transport, Chem. Eng. Sci., **60** (2005) 815–826.

16 R. Grossier, A. Magnaldo, S. Veesler, Ultra-fast crystallization due to confinement, J. Cryst. Growth **312** (2010) 487–489.

17 J. Zhao, H. Miao, L. Duan, Q. Kang, L. He, The mass transfer process and the growth rate of NaCl crystal growth by evaporation based on temporal phase evaluation, Opt. Lasers Eng. **50** (2012) 540–546.

18 N. Shahidzadeh, J. Desarnaud, Damage in porous media: role of the kinetics of salt (re)crystallization, Eur. Phys. J. Appl. Phys. **60** (2012) 24205.

19 J. Crank, *The mathematics of diffusion*, Oxford University Press, Second edi., 1975.